JET-R(95)02

Extension of a Bohm Model for L-mode Electron Heat Transport to Ion Heat Transport and to the Ohmic Regime

M Erba, V Parail, E Springmann, A Taroni.

JET Joint Undertaking, Abingdon, Oxfordshire, OX14 3EA, UK.

February 1995

ABSTRACT

The results of simulations of several JET L-mode and ohmic discharges performed with a Bohm-like expression for both ion and electron thermal diffusivities are presented. Comparisons with experimental ion and electron temperature profiles of auxiliary heated discharges show that χ_i has to be at least twice larger than χ_e to simulate the L-mode regime even for shots with dominant electron heating . Simulations of ohmic discharges with currents ranging from 1 to 7 MA show that the Bohm-like model for L-mode has to be preferred to a Neoalcator-like expression of the electron thermal diffusivities.

1) INTRODUCTION

A family of empirical models of the Bohm type for the simulation of L-mode discharges in JET was derived in [1]. The simplest of these models , allowing good simulations of a series of reference discharges is given in the following expressions , where 'a' is the minor radius and for the other quantities we use standard notations :

$$\chi_e = \alpha_e \ \chi_B \ q^2 \ / \ L_p^* \qquad (1)$$

$$\chi_i = \alpha_i \ \chi_e \ + \ \chi_{neocl} \qquad (2)$$

$\chi_B = ckT_e/eB_0$ is the Bohm diffusivity coefficient in cgs units , the numerical factors are $\alpha_e = 3.3 \cdot 10^{-4}$, $\alpha_i = 1$, the dimensionless quantities are $L_p^* = (dp/dr)^{-1}$ p/a and the safety factor q while χ_{neocl} is the neoclassical ion diffusivity.

In the discharges considered in [1] (ρ^*-scaling experiments [2] , on-axis/off-axis ICRH heating experiments [3] , current ramp experiments [4]) only electron temperature profiles were available because NBI heating had not been used and for this reason the Charge Exchange Recombination diagnostic [5] for T_i was not available. Thus only the expression for electron diffusivity χ_e could be tested in this preliminary analysis, and it was assumed that $\alpha_i = 1$.

The choice $\alpha_i = 1$ was based on the observation that ion energy transport appears in general to be of the same order as the electron transport , but this approach was not justified by simulations of discharges where both T_i and T_e were experimentally available and a separation of the contribution to the heat fluxes from the electron and the ion channel is possible.

In this paper we try to model both ion and electron transport by simulating a set of L-mode discharges chosen in the JET data-base where the experimental ion temperature profiles are available.

In our approach we start from the observation that the results of TRANSP analysis of ordinary L-mode JET discharges indicate that $\chi_i > \chi_e$ all over the plasma column [6]. Hence we keep on using eq. (2) for χ_i and increase the value of α_i trying to optimize the agreement with experimental results. By making this choice we are implicitly assuming the ratio χ_i / χ_e to be constant within the range of variation of plasma parameters in our set of selected discharges (from Tables I and II it can be seen that only average density and input power vary significantly). The parametric dependences of χ_e in our model have been studied in [1] .

Another important issue is the confinement in the ohmic regime observed in JET: old analysis of JET data [7] , recent results from ASDEX [8] , TORE SUPRA [9] and ALCATOR C-MOD [10] suggest that when the density is too high the confinement time stops rising linearly with density as prescribed by the so-called Neo-Alcator scaling law [11] and saturates. The saturated ohmic regime possesses many features similar to the L-mode regime (like confinement degradation with power), and a model for L-mode might describe successfully ohmic discharges (at least in their density saturated regime, commonly observed in large machines). In this paper we will report results of simulations of ohmic JET cases with various currents and densities carried out with our Bohm model showing that this is indeed the case. For comparison the same ohmic discharges were also simulated with a

Neoalcator-like electron thermal diffusivity [12] giving much worse results in terms of both local and global quantities.

2) DESCRIPTION OF THE MODEL

In the following we shall use an already tested version of the Bohm model (eqs. (1),(2)) with various choices of the numerical factors α_i , α_e in the expressions for ion and electron thermal diffusivities. Three different sets of α_e , α_i were used to test how much larger is χ_i than χ_e:

$$\alpha_e = 3.3 \cdot 10^{-4} \quad , \quad \alpha_i = 1.0 \tag{3}$$

$$\alpha_e = 2.6 \cdot 10^{-4} \quad , \quad \alpha_i = 2.0 \tag{4}$$

$$\alpha_e = 2.1 \cdot 10^{-4} \quad , \quad \alpha_i = 3.0 \tag{5}$$

Eq. (3) was used in previous simulations [1]. Eq. (4) describes approximately the same global confinement as eq. (3) , but ion diffusivity is twice larger than electron diffusivity and finally eq. (5) is similar to eq. (4) , but the ion thermal diffusivity is three times larger than electron one.
Note that α_e has been decreased in eqs. 4) and 5) as α_i has been increased with respect to eq. (3) in order to keep global confinement constant .
The possibility of telling these models apart relies on the availability, in the JET database, of well diagnosed L-mode discharges where experimental profiles of T_i and T_e are available . In particular it is interesting to study the behaviour of the models when the parameter T_e/T_i varies significantly.

3) L-MODE TRANSPORT SIMULATIONS

We consider a set of 6 well-diagnosed quasi-stationary L-mode JET discharges. We exclude from our analysis special confinement regimes such as the Hot-Ion L-mode [13] and the Pellet Enhanced Confinement (PEP) [14] regimes observed at JET which might possess confinement properties different from ordinary L-mode discharges.
In Table I we report the parameters of the cases studied. The total input power and its distribution between the ions and the electrons in these cases is specified in Table II.

The set of simulated L-mode discharges includes cases with current of 3 MA and toroidal field of approximately 3 T for which it has been possible to find in the JET data-base a complete set of experimental profiles required for simulation. However the overall dependence of the model on these parameters had been tested in ref. [1] using the ρ^*-scaling [2] and current ramp [4] experiments.
Electron temperature profiles have been measured with the Electron Cyclotron Emission diagnostic (ECE) [15] and with the LIDAR [16] Thompson scattering measurement ; ion temperature profiles have been measured using the Charge Exchange Recombination diagnostic (CXSM) [5]. Data for ion temperatures are only available during Neutral Beam Operation: hence only cases with Neutral Beam Heating, or combined Neutral Beam and Ion Cyclotron Heating have been considered. Typical error bars of experimental temperature profiles are given in the figures.
All these discharges have been simulated during an L-mode, quasi-stationary phase. The simulations have been carried out in a semi-predictive way using the JETTO transport code [17] : only heat diffusion has been modelled, while interferometric density profiles and the Z_{eff} profile, measured using Charge Exchange Recombination diagnostic (when available : otherwise an average brehmsstrahlung measurement has been used), have been imposed throughout the time evolution.
When necessary we have modelled the effect of sawteeth by increasing the value of the diffusion coefficient in the region within the inversion radius.
In the case of discharges # 19642 and # 16047 the profiles given by the PION code [18] have been used for the deposition profiles of ICH power. NBI deposition profiles given by TRANSP [19] have been used for discharges 19691 and 19649. In other cases we have used deposition profiles , obtained with the code PENCIL [20], which is linked to JETTO.
Discharges 19649 and 19691 are those for which the best NBI power deposition profiles are available from TRANSP analysis. For both shots eq. (6) clearly underestimates ion transport in the centre. The results of TRANSP analysis of this discharge also indicate that $\chi_i > \chi_e$ [6].

In all other simulated cases we also found that the best agreement with experiment is obtained when the coefficients are chosen according to eq. 4) (see figs. 1-6) .
So far we analysed discharges with predominant ion heating. Discharge # 16047 is of particular interest because in this case the electron temperature is higher than the ion temperature thanks to the use of ICRH auxiliary power , and the validity of the choice $\chi_i = 2\,\chi_e$ is tested for values of the parameter T_e/T_i larger than 1 . The simulations are satisfactory also in this case using the coefficients described in eq. 4) or 5) , while the choice $\chi_i = \chi_e$ (eq. 3)) leads to an overestimation of ion temperature profiles well outside the error bars.

We conclude that the choice $\chi_i = \chi_e$ underestimates ion transport in JET L-mode discharges independently of the heating method, and better results are obtained using models with $\chi_i = 2\text{-}3 \cdot \chi_e$ (the model with $\chi_i = 2\,\chi_e$ performs marginally better). A quantitative confirmation of this result can be obtained through statistical analysis (see section 5)).

4) RESULTS OF THE SIMULATION OF THE JET OHMIC REGIME AT VARIOUS PLASMA CURRENTS AND DENSITIES

We will now present the results of the simulation of the ohmic phase of a group of JET discharges performed using the Bohm model with the value of the numerical coefficients given by eq. 4) (the one giving best results in the simulation of ion and electron temperatures in L-mode). These discharges have been selected in order to test the dependence of transport on the safety factor q and on density.
In Table V we report the parameters of these discharges , for which only experimental electron temperature profiles are available in the JET data-base.
Simulations are carried out towards the end of the current flat top : at these times the loop voltage on axis and the surface voltage are similar , indicating that the diffusion of the poloidal field is nearly complete and a steady state has been reached.
We will try both the Bohm model with the choice of the coefficients given by eq. (7) , and a Neo-Alcator-like model [12] :

$$\chi_e^{N.A.} \equiv \varepsilon \frac{c^2}{\omega_{pe}^2} \frac{v_{the}}{qR} \frac{r}{R} \qquad (6)$$

In eq. (6) ε is a numerical constant , $\omega_{pe} = \sqrt{4\pi n_e e^2/m_e}$ is the plasma frequency, $v_{the} = \sqrt{2T_e/m_e}$ is the electron thermal velocity , q is the safety factor, r is the radial coordinate, R is the major radius. When the neoalcator coefficient is used for electron thermal conduction , a purely neoclassical expression is applied to the ions, as suggested in [21].
The above expression provides a scaling for the confinement time with a linear dependence on density. This model has been used in predictive simulations of L-mode discharges in combination with a gyro-Bohm-like expression of the thermal diffusivity [22] (with $\varepsilon = 0.71$).

In order to make a comparison between our Bohm model and the Neo-Alcator model we have chosen the value of the constant $\varepsilon = 6.3$ in front of the diffusivity given by eq. 6) : in this way the thermal electron energy is normalized to the experimental value measured in the reference shot 27588. However we point out that with this choice ε is much larger than the value used in reference [22]. In the case of the Bohm model on the other hand, we are able to obtain good results using the same values of the coefficients already used in the simulation of L-mode discharges.

In Table VI the thermal electron energy content resulting from the neoalcator model is shown together with the thermal energy content resulting from the Bohm model and the kinetic electron energy obtained from experimental electron temperature and density profiles.

As it can be seen, the neoalcator-like model, although normalized in order to obtain the experimental value of W_{the} in the reference case 27588, fails in the low current , low density shot 25255. On the other hand the Bohm model gives results which reproduce the kinetic energy with an accuracy within the 20 % level in all selected discharges (this is the error level related to the measurement of kinetic energy [23] at JET) . We can conclude that transport analysis of ohmic JET discharges rules out the model for electron transport, while good results can be obtained with the neoalcator-like model used for L-mode confinement.

It is worth mentioning that starting from the definitions of our local models eqs. (1),(2) and (6), it is possible to derive scaling laws for the electron thermal energy in the ohmic regime using the power balance equation. This is similar to what has been done in reference [1] for the thermal energy confinement time in the L-mode regime, even though in the ohmic regime the input power is not a free parameter and can be expressed in terms of the current and the resistivity. For the Bohm-like models we obtain:

$$W_{the}^{Bohm} = C_{Bohm} \cdot R^{11/7} \cdot a^{2/7} \cdot I^{8/7} \cdot \langle n \rangle^{5/7} \cdot B^{-2/7} \cdot \langle Z_{eff} \rangle^{2/7} \qquad (7)$$

while for the N.A. model we get:

$$W_{the}^{N.A.} = C_{N.A.} \cdot R^{4/3} \cdot a^{5/3} \cdot I^{1/3} \cdot \langle n \rangle \cdot B^{1/3} \cdot \langle Z_{eff} \rangle^{2/7} \qquad (8)$$

By using shot 27588 as a normalization case, we deduce the following values of the coefficients C_{Bohm} and $C_{N.A.}$:

$$C_{Bohm} = 1.258 \cdot 10^{-1} \quad , \qquad C_{N.A.} = 9.281 \cdot 10^{-2} \qquad (9)$$

with R(m), a(m) , I(MA) , B(T) , <n> (10^{20} m^{-3}) , W_{the}(MJ) in eqs. (9),(10) (in place of the minor radius 'a' we use the equivalent radius ρ_{max} resulting from experimental equilibria and R=3.10 m).
With this choice of C_{Bohm} and $C_{N.A.}$ it is possible to reproduce approximately the values of W_{the} resulting from numerical computation (shown in Table VI). From eqs. (7) and (8) it appears that the main differences between the N.A. and Bohm scalings are the current and density dependences: the N.A. model fails because experimental data support a linear scaling with current and do not follow a linear dependence on density.
We also observe that the overall dependence on dimensions would be stronger in the N.A. model , due to a strong dependence on a , not observed in standard scaling laws.
Our local predictive calculations also allow us to compare the computed temperature profiles with the measured ones: in fig. 7 we show the comparison between profiles obtained with the N.A. model, with the Bohm model and with experimental profiles. It can be seen that the N.A. model gives "parabolic" temperature profiles which compare badly with the experimental ones. The Bohm model also describes the transient phase between Ohmic and L-mode confinement regimes accurately , during which the plasma is heated by the onset of auxiliary input power. This is illustrated in fig. 8 where the evolution of the electron thermal energy content for the case of discharge 24693 is shown (I_p=3.1 MA , $\langle n_e \rangle \approx 0.3 \cdot 10^{20}$ m^{-3} , B_t = 2.8 T , $\langle Z_{eff} \rangle \approx 2.0$) .

5) STATISTICAL ANALYSIS OF SIMULATIONS RESULTS

It is important to have a means to assess the validity of a model that can be applied to a number of simulations on a statistical basis rather than on visual comparison of computed and experimental profiles .
This analysis should tell us in an objective way the limits of confidence in the predictions of our model.
We adopt a simplified version of the approach followed by Kinsey et al [24] for the statistical analysis of results of predictive simulations of local transport properties. We assume that the probability density for obtaining the j^{th} radial measurement of the i^{th} profile is defined as:

$$p_{ij} = \frac{1}{\sqrt{2\pi\Delta_i^2}} e^{-(\varepsilon_{ij} - m_i)^2 / 2\Delta_i^2} \qquad (10)$$

ε_{ij} represents an expression for the deviation of computation results from experimental data defined as :

$$\varepsilon_{ij} \equiv \frac{X_{ij} - Y_{ij}}{Y_{ij}} \qquad (11)$$

where X_{ij} is the computed quantity at the j-th radial point of the i-th profile and Y_{ij} is the experimental quantity at the j-th radial point of the i-th profile. m_i corresponds to corrections for calibration/modelling offsets common to each profile but differing from one profile to another one , while Δ_i is the measurement variance. We assume these quantities to be independent of the radial position j , i.e. we are considering errors to be radially uniform.
By maximizing the probability of obtaining the complete set of deviations $\{\varepsilon_{ij}\}$ we get for the i^{th} profile :

$$m_i = \frac{\sum_1^{N_i} j \, \varepsilon_{ij}}{N_i} \qquad (12)$$

$$\Delta_i^2 = \frac{\sum_1^{N_i} j \, (\varepsilon_{ij} - m_i)^2}{N_i} \qquad (13)$$

being N_i the number of radial points .
Since in our computations we only model heat transport we will compute these quantities for temperature only (X=T). We obtain for each profile:

$$m \equiv \frac{\sum_{1}^{N} j \left(\left(T_{exp}(x_j) - T(x_j) \right) / T(x_j) \right)}{N} \qquad (14)$$

$$\Delta^2 \equiv \frac{\sum_{1}^{N} j \left(\left(T_{exp}(x_j) - T(x_j) - m \right) / T(x_j) \right)^2}{N} \qquad (15)$$

where T_{exp} is the measured value of the electron or ion temperature , T is the temperature computed with a given model and x = r/a ; the sum is extended over a selected group of radial points (N~10), chosen inside the so-called transport dominated region (q > 1 , x < 0.9) where meaningful tests can be carried out without taking into account an accurate description of sawtooth activity and atomic physics processes. Given the scope of this work , no attempt is made to validate the model outside this region.
In Table III and IV we show the results of the numerical computation of m and Δ for electron and ion temperatures resulting from the coefficients choices given in eqs. 3) , 4) and 5) in the case of L-mode discharges. We observe that eq. 3) gives values of m and Δ in many cases greater than 10 % , while the smallest values are usually obtained with eq. 4) (this in particular is true for the discharges analysed with TRANSP , #19649 and #19691). These calculations confirm the tendency of eq. 4) to give best results in L-mode shots for ion transport , even though eq. 5) is also very close to the data and cannot be ruled out.
In Table VII we report the values obtained for m and Δ when using for T the electron temperature computed with the N.A. model and the Bohm model for the simulated ohmic discharges (the corresponding computed and experimental profiles are shown in fig. 7)).
Also in this case results are in agreement with what had been qualitatively deduced in section 4) : the overall level of transport and temperature profiles are much better simulated with the Bohm model rather than with the N.A. model alone.

6) CONCLUSIONS

In this paper we have discussed the results of simulations of JET experiments starting from the Bohm-like model for local electron heat confinement first proposed in [1].
The simulation of a selection of L-mode discharges where T_i measurements are available has shown that the Bohm model with $\chi_i = 2\text{-}3 \cdot \chi_e$ is able to

reproduce both electron and ion temperature profiles. Our results are in agreement with TRANSP analysis carried out on a subset of the L-mode discharges studied here. However it has not been possible to test different scalings of χ_i with respect to χ_e due to the limited variation of plasma parameters. Another interesting result is that ohmic discharges in JET can be described with the same model used for L-mode. This implies that the neoalcator scaling is not valid in JET ohmic discharges which appear to be well inside the regime of saturated density dependence typical of large experiments.

ACKNOLEDGEMENTS

We wish to thank D.V. Bartlett , A. Cherubini , J.G. Cordey and M. Von Hellermann for useful comments and discussions , B. Balet for providing the results of TRANSP analysis and L.G. Eriksson for providing the PION deposition profiles used in the simulations presented in this paper.

REFERENCES

[1] Taroni A., Erba M., Tibone F., Springmann E., Plasma Phys. Control. Fusion **36** (1994) 1629 .

[2] Christiansen J. P. , et al. , Nucl. Fus. **33** (1993) 863.

[3] Cordey J G et al, 1992 Proceedings of the 14th Int. Conf. on Plasma Physics and Controlled Nuclear Fusion Research, IAEA-CN-56/D-3-4,Wurtzburg 1992, IAEA, Vienna.

[4] Challis C.D. , et al. , Nucl. Fus. **32** (1992) 2217.

[5] Weisen H. , Von Hellermann M. , Boileau A. , et al. , Nucl. Fus. **29** (1989) 2187.

[6] Balet B. , Cordey J.G. , Stubberfield P.M. , Plasma Phys. Contr. Fusion **34** (1992) 3.

[7] Cordey J.G., 'Energy confinement in JET ohmically heated plasma', JET Report JET-R(87)02.

[8] Bessenrodt-Weberpals M. et al., Nucl. Fus. **31** (1991) 155.

[9] Garbet X. , Payan J. , Laviron C. , et al. , Nucl. Fus. **32** (1992) 2147

[10] Porkolab M. , Bovin R. , Bombarda F. , et al. , 'Overview of recent results from Alcator C-MOD' , IAEA Paper CN-60/A-1-II-2 , 15th International Conference on Plasma Physics and Controlled Nuclear Fusion Research , Seville , Spain , 1994.

[11] Goldston R.J., Plasma Phys. and Contr. Nucl.Fus. **26**,1A(1984) 87.

[12] Horton W., Choi O.I., Yushmanov P.N., Parail V.V., Plasma Phys. Contr. Fus. **29** (1987) 901.

[13] Balet B. , Boyd D.A. , Campbell D.J. , et al. , Nucl. Fus. **30** (1990) 2029 .

[14] Taroni A. , Balet B. , Betello G. , et al. , "Global Power Balance and Local Heat Transport in JET" IAEA paper CN-50/A-VII-1 , Proceedings of the 12th Int. Conf. on Plasma Physics and Contr. Fus. Res. , Nice , 1988.

[15] Costley A.E. , Baker E.A.M. , Bartlett D.V. , et al. , in Controlled Fusion and Plasma Physics Vol.9F , Part I , European Physical Society (1985) 227.

[16] Salzmann H. , Bundgaard J. , Gadd A. , et al. , Rev. Sci. Instrum. **59** (1988) 1451.

[17] Cenacchi G., Taroni A., "JETTO : A Free-Boundary Plasma Transport Code (Basic Version)" , Rapporto ENEA RT/TIB 88(5) 1988.

[18] Eriksson L.G., Hellston T., Willen U., Nucl. Fus **33** (1993) 1037.

[19] Goldston R. J. , McCune D.C. , Towner H.H. , et al. , J. Comp. Phys. **43** (1981) 61.

[20] G. Corrigan , D.G. Muir , F. Tibone , "Neutral Beam-Plasma Interaction in JET : Comparison of PENCIL and TRANSP Modelling Results" , JET-R(91)14.

[21] Merezhkin V.G. and Mukhovatov V.S., JETP Lett, **33** (1981) 446.

[22] Parail V.V. and Yushmanov P.N., Proceedings 12th Conference on Plasma Physics and Controlled Nuclear Fusion, Nice, Vol.2 (1988) 3 .

[23] Watkins M.L. and Keilhacker M. , " The Normal Level of Accuracy of PPF Data ", JET Report JET-IR(88) 12 .

[24] Kinsey J. , Singer C. , Djemil T. , Cox D. , Bateman G. , "Systematic Comparison of a Theory-based Transport Model with a Multi-tokamak Database" , poster presented at the Workshop "Transport in Fusion Plasmas" , Aspenas , Goteborg , Sweden 1994.

TABLE I

TABLE I) : Plasma parameters values of the simulated L-mode discharges.

DISCHARGE	$\langle n_e \rangle_{20}$	$\langle Z_{eff} \rangle$	I_p (MA)	B_t (T)
19649	0.28	2.4	3.0	3.0
19691	0.39	3.7	3.0	3.0
24693	0.33	2.1	3.1	2.8
26109	0.20	3.0	3.1	2.8
19642	0.55	3.7	3.0	3.1
16047	0.28	2.2	3.0	3.1

TABLE II

TABLE II) : Values of NBI heating power , ICRH heating power and ohmic heating power of the simulated L-mode discharges.

shot, time	P_{TOT}	P_{NBE}	P_{NBI}	P_{RFE}	P_{RFI}	P_{OH}
19649	10.4	3.0	5.8	-	-	1.6
19691	17.5	5.5	10.5	-	-	1.5
24693	8.6	4.1	3.5	-	-	1.0
26109	5.3	2.0	1.8	-	-	1.5
19642	14.9	2.9	2.4	4.0	3.8	1.8
16047	10.7	1.1	2.9	4.1	1.8	0.8

TABLE III

TABLE III) : Values of the linear deviation m and the mean square root deviation Δ of computed electron temperature profiles with respect to experimental electron temperature profiles for L-mode cases.

Shot Number	$m_e(\%)$ $\alpha_i=1$	$m_e(\%)$ $\alpha_i=2$	$m_e(\%)$ $\alpha_i=3$	$\Delta_e(\%)$ $\alpha_i=1$	$\Delta_e(\%)$ $\alpha_i=2$	$\Delta_e(\%)$ $\alpha_i=3$
19649	0.82	-2.7	-3.1	6.4	7.1	7.3
19691	7.1	7.8	7.2	8.7	9.4	9.1
24693	2.1	2.3	3.9	4.7	4.3	5.1
26109	-4.0	-2.5	-2.1	4.5	3.1	2.8
19642	2.0	1.7	1.5	6.0	7.4	8.5
16047	-2.0	4.1	8.1	3.4	5.9	9.6

TABLE IV

TABLE IV) : Values of the linear deviation m and the mean square root deviation Δ of computed ion temperature profiles with respect to experimental ion temperature profiles for L-mode cases.

Shot Number	$m_i(\%)$ $\alpha_i=1$	$m_i(\%)$ $\alpha_i=2$	$m_i(\%)$ $\alpha_i=3$	$\Delta_i(\%)$ $\alpha_i=1$	$\Delta_i(\%)$ $\alpha_i=2$	$\Delta_i(\%)$ $\alpha_i=3$
19649	13.2	1.1	-5.0	13.5	2.5	5.3
19691	8.4	2.5	-2.5	10.5	5.7	5.3
24693	3.8	-2.9	-5.7	5.6	4.3	7.0
26109	11.0	2.0	-4.6	12.8	5.2	5.8
19642	4.4	-2.6	-8.6	8.5	6.0	9.7
16047	23.4	0.39	-17.7	23.8	2.1	17.8

TABLE V

TABLE V) : Plasma parameters values of the simulated ohmic discharges.

DISCHARGE	$\langle n_e \rangle 20$	$\langle Z_{eff} \rangle$	I_p (MA)	ρ_{max} (m)	B_t (T)
25255	0.10	2.5	1.0	1.4	2.8
27658	0.17	3.7	2.05	1.5	1.7
27588	0.30	3.3	3.3	1.5	2.8
20050	0.37	1.3	5.1	1.5	3.1
27897	0.28	2.3	7.0	1.6	3.3

TABLE VI

TABLE VI) : Total thermal energy resulting from computations carried out with the Bohm model and the neoalcator-like model compared with experimental values.

DISCHARGE	W_{the}(MJ) Bohm	W_{the}(MJ) N.A.	W_{kin}(MJ) exp	Ratio Bohm/exp	Ratio N.A./exp
25255	0.13	0.19	0.11	1.2	1.7
27658	0.53	0.45	0.52	1.2	0.86
27588 , ref	1.05	1.05	1.05	1.0	1.0
20050	1.7	1.2	1.9	0.89	0.63
27897	1.9	1.5	1.9	1.0	0.79

TABLE VII

TABLE VII) : Values of the linear deviation m and the mean square root deviation Δ of computed electron temperature profiles with respect to experimental electron temperature profiles for Ohmic cases.

DISCHARGE	m(%) N.A.	m(%) Bohm	Δ(%) N.A.	Δ (%) Bohm
25255	8.2	1.0	30.4	8.7
27658	-34.6	-3.5	39.7	7.5
27588	-10.5	-10.9	23.9	15.5
20050	-25.3	1.5	40.0	7.1
27897	-25.2	3.5	31.8	5.0

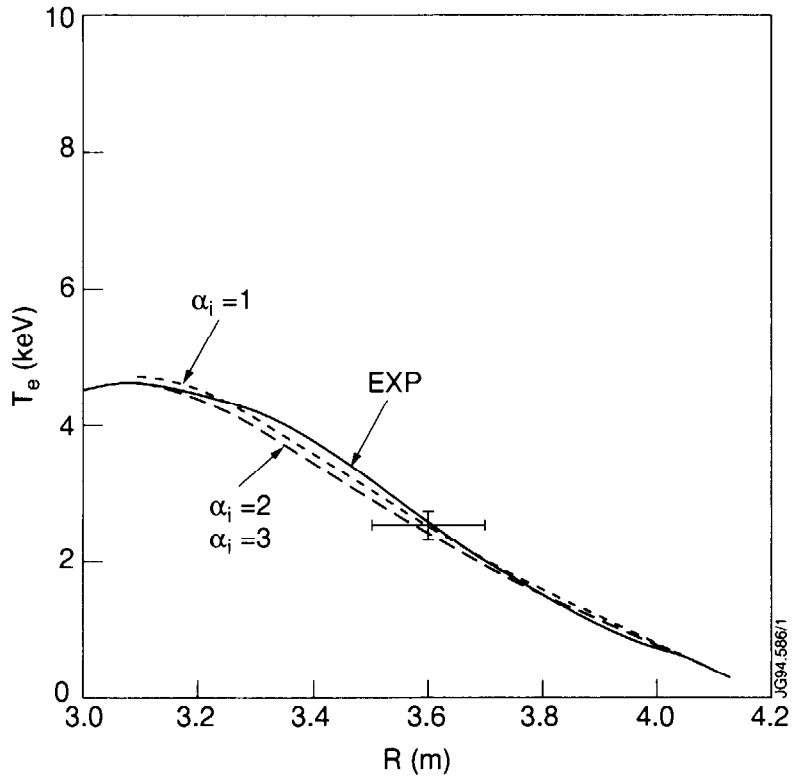

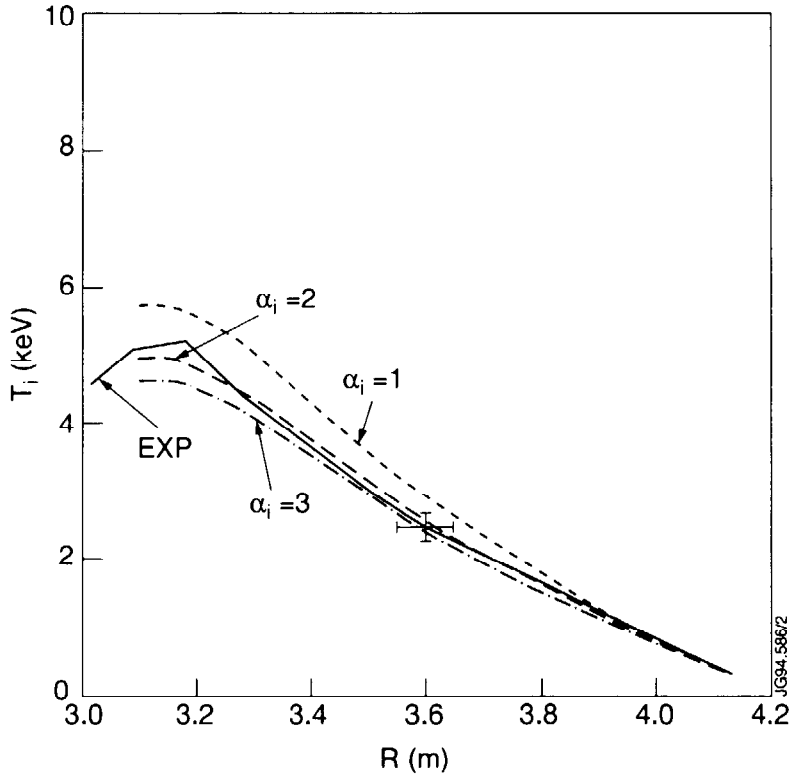

FIGURE 1) : Electron a) and ion b) temperature profiles obtained using α_i=1,2,3 compared with experimental profiles for discharge 19649. At R=3.6 m experimental error bars are shown for both the temperature and the radial position.

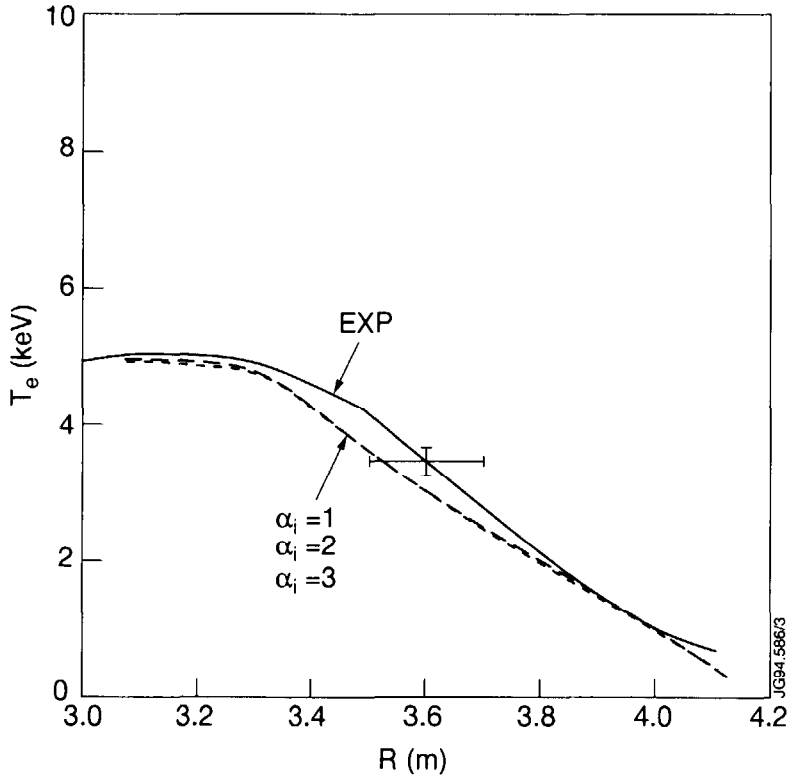

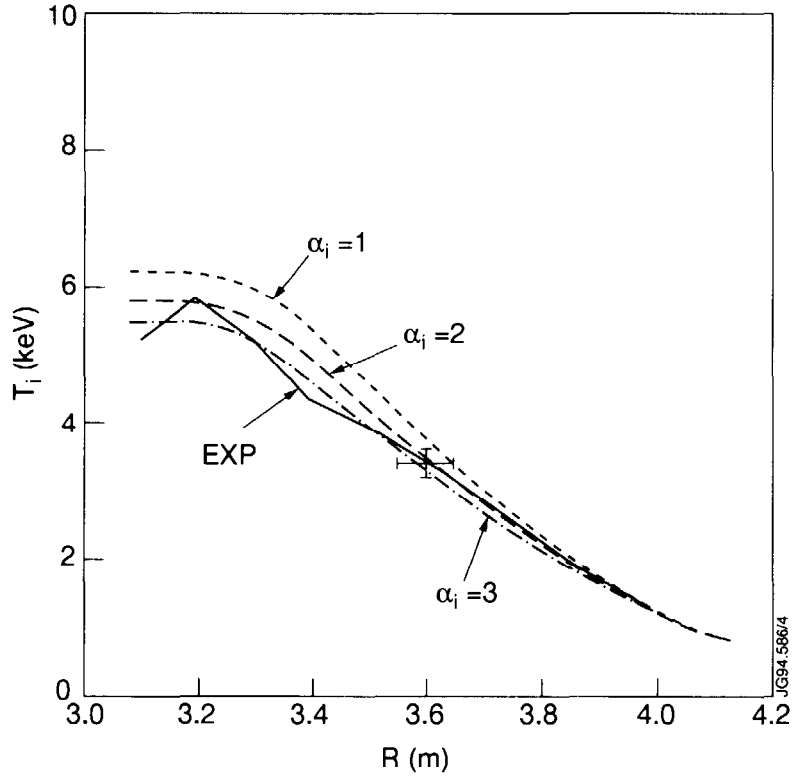

FIGURE 2) : Electron a) and ion b) temperature profiles obtained using α_i=1,2,3 compared with experimental profiles for discharge 19691. At R=3.6 m experimental error bars are shown for both the temperature and the radial position.

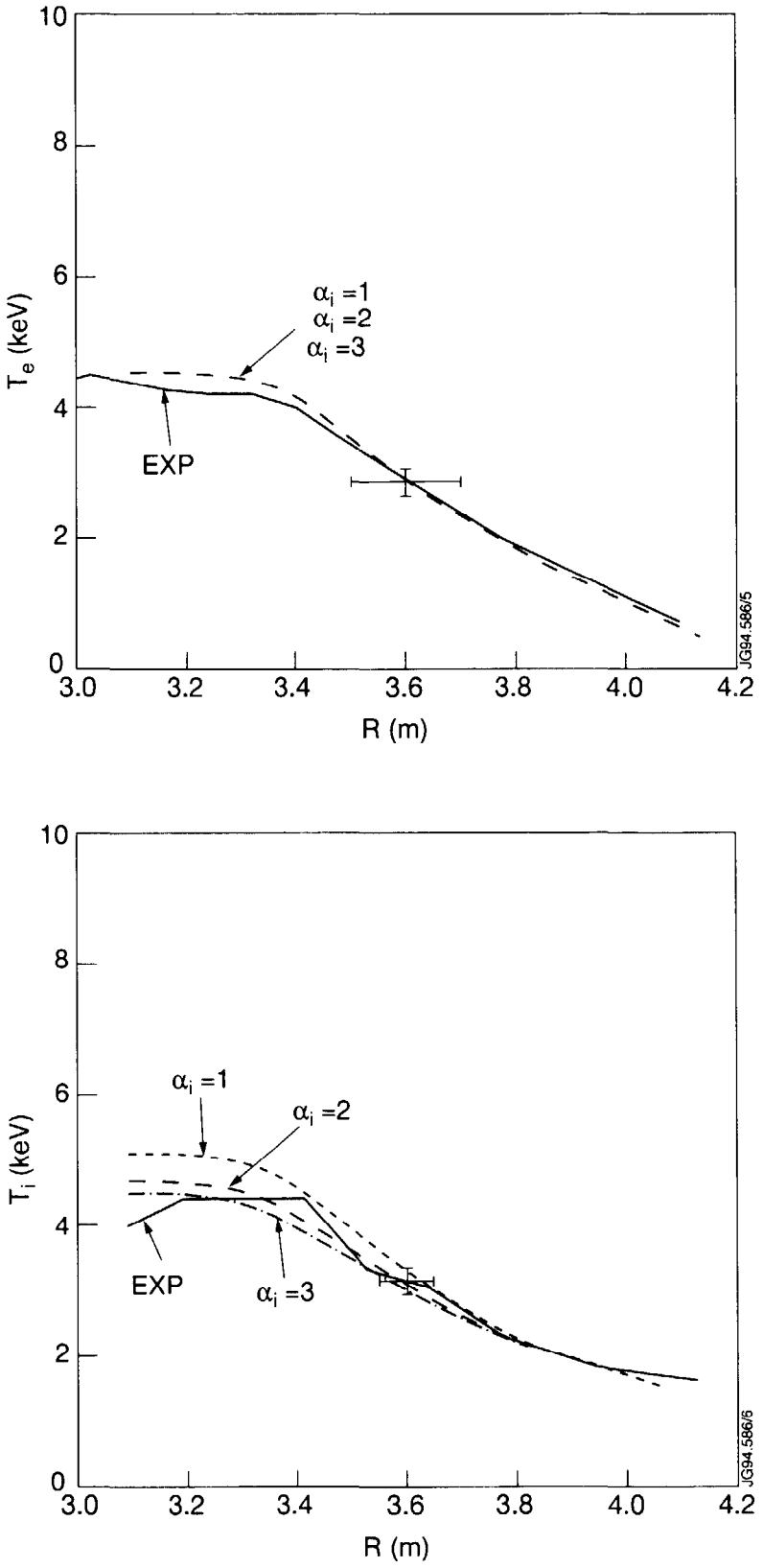

FIGURE 3) : Electron a) and ion b) temperature profiles obtained using α_i=1,2,3 compared with experimental profiles for discharge 24693. At R=3.6 m experimental error bars are shown for both the temperature and the radial position.

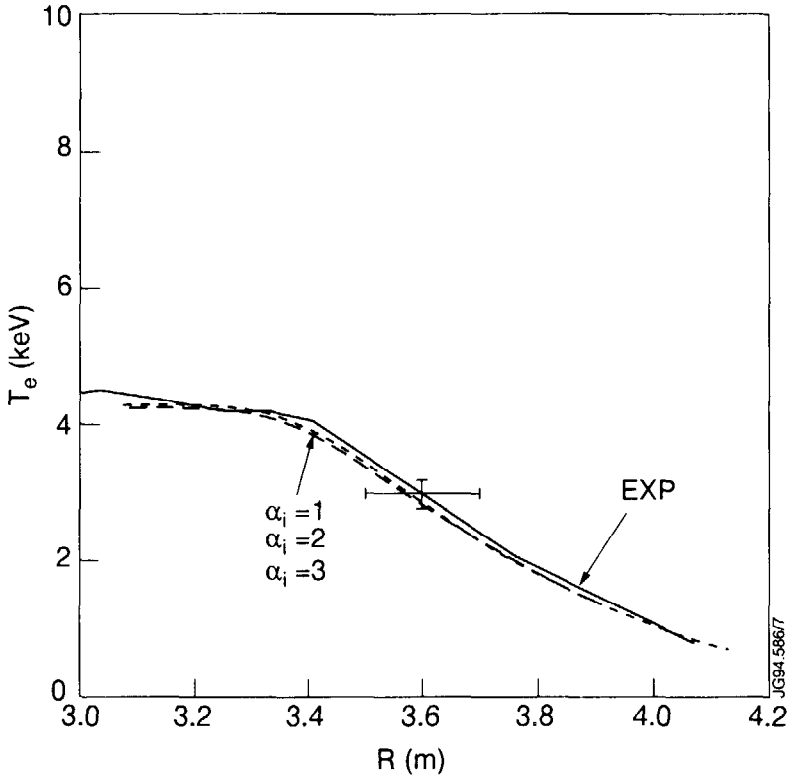

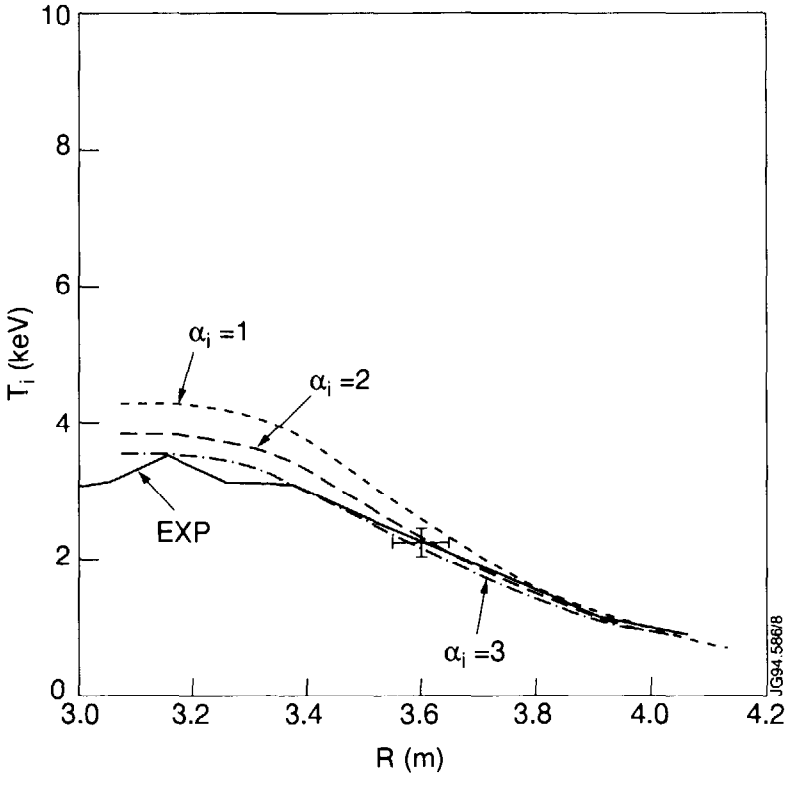

FIGURE 4) : Electron a) and ion b) temperature profiles obtained using α_i=1,2,3 compared with experimental profiles for discharge 26109. At R=3.6 m experimental error bars are shown for both the temperature and the radial position.

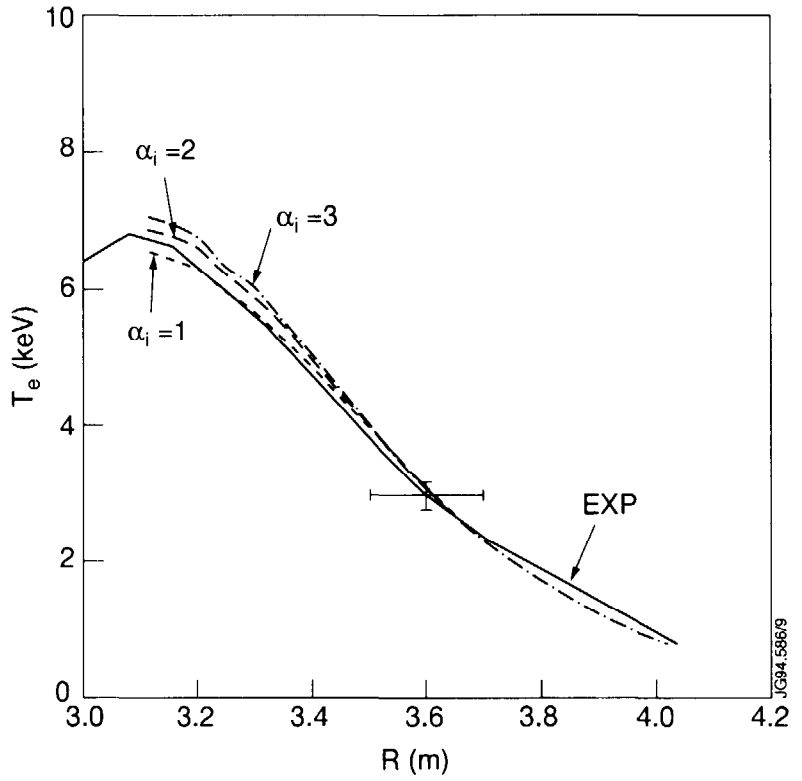

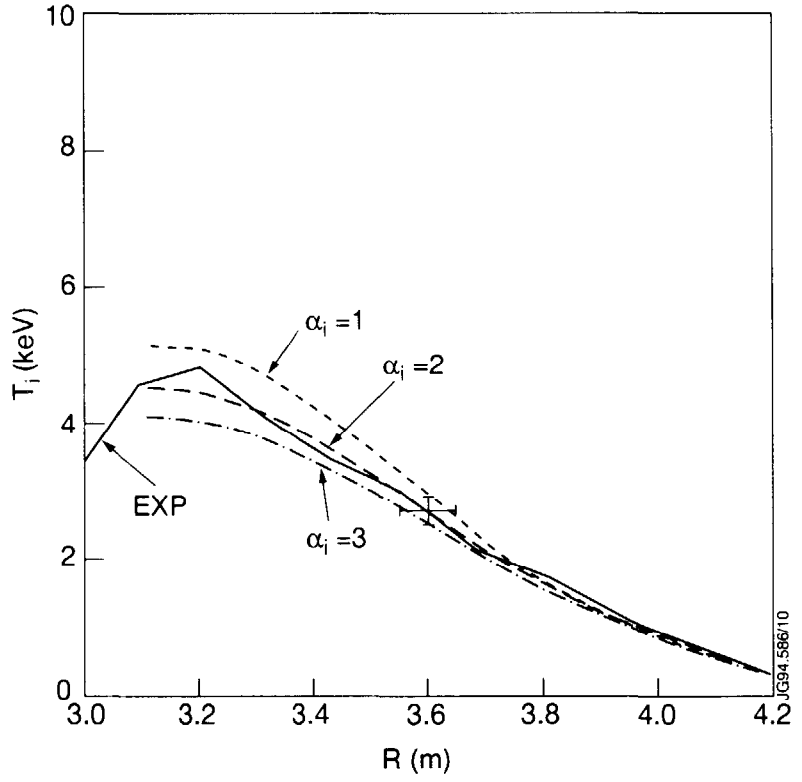

FIGURE 5) : Electron a) and ion b) temperature profiles obtained using α_i=1,2,3 compared with experimental profiles for discharge 19642. At R=3.6 m experimental error bars are shown for both the temperature and the radial position.

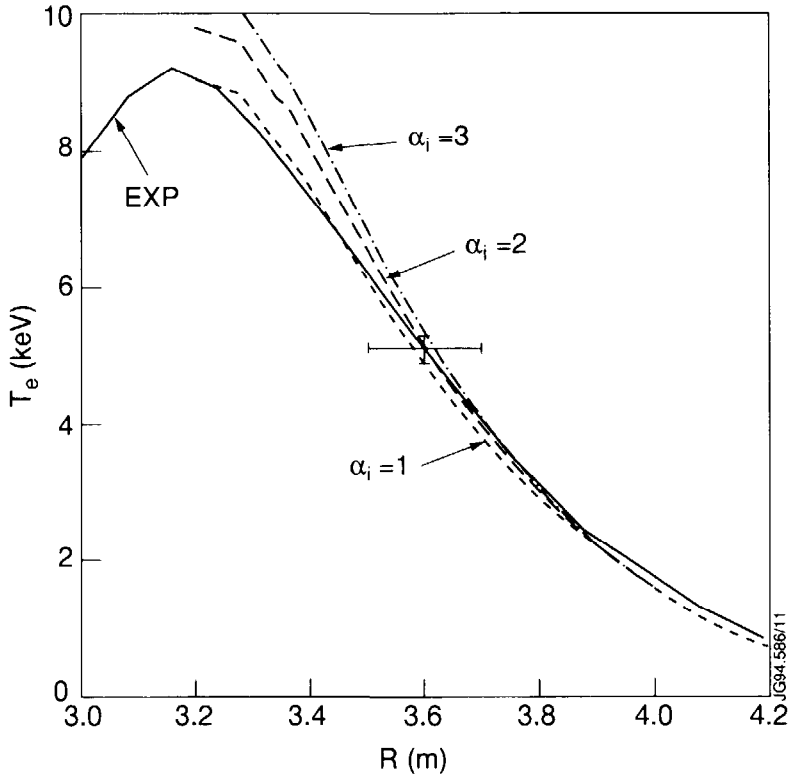

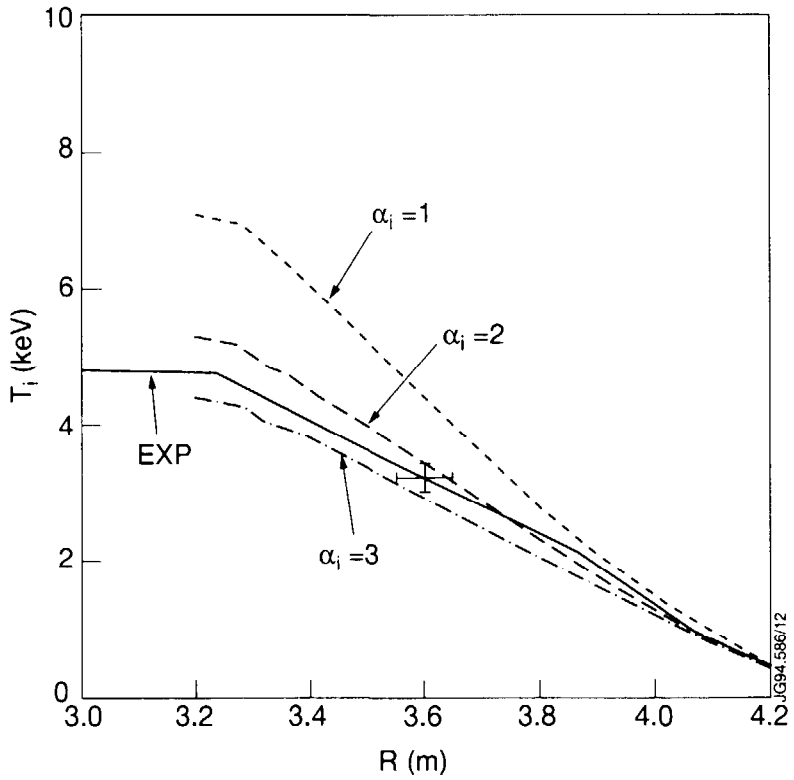

FIGURE 6) : Electron a) and ion b) temperature profiles obtained using α_i=1,2,3 compared with experimental profiles for discharge 16047. At R=3.6 m experimental error bars are shown for both the temperature and the radial position.

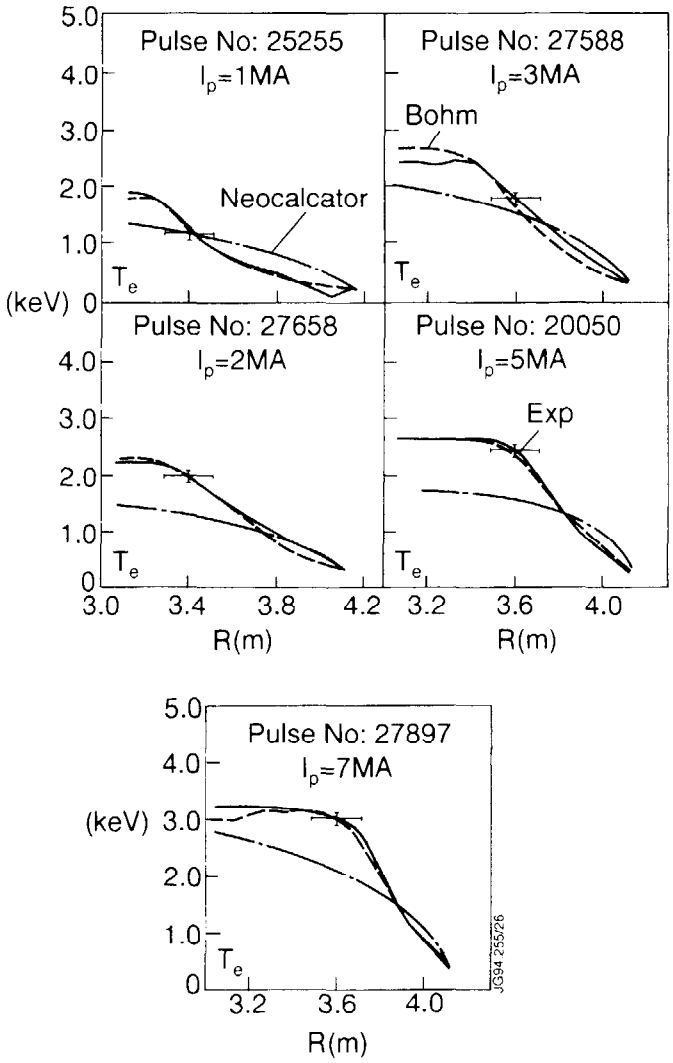

FIGURE 7) : Electron temperature profiles resulting from the Bohm and from the neoalcator-like model compared with experimental profiles for the ohmic phase of discharges 25255 , 27588 , 27658 , 20050 and 27897. Error bars are shown for both the temperature and the radial position.

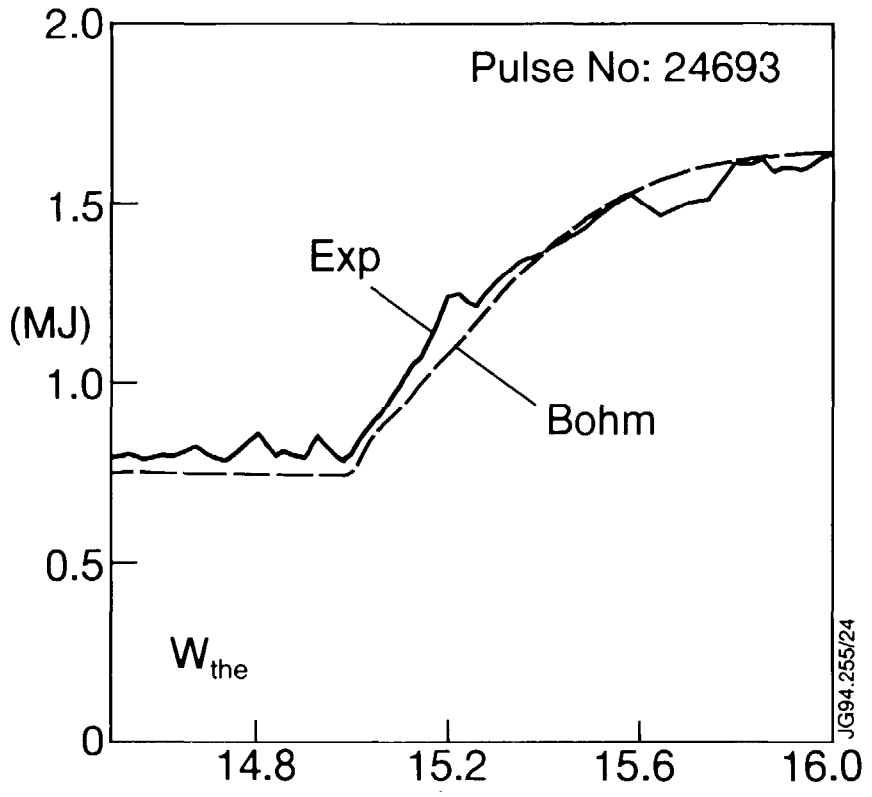

FIGURE 8) : Time evolution of total thermal energy obtained with the Bohm model compared with the time evolution of the experimental kinetic energy.